

ARMY RESEARCH LABORATORY



**Experimental Measurement and Computational Simulation  
of the Strains on a Single Yarn in a Kevlar Fabric  
During Stretching**

**by Jian H. Yu, Brandon McWilliams,  
Peter G. Dehmer, and Chian-Fong Yen**

**ARL-TR-5224**

**June 2010**

## **NOTICES**

### **Disclaimers**

The findings in this report are not to be construed as an official Department of the Army position unless so designated by other authorized documents.

Citation of manufacturer's or trade names does not constitute an official endorsement or approval of the use thereof.

Destroy this report when it is no longer needed. Do not return it to the originator.

# **Army Research Laboratory**

Aberdeen Proving Ground, MD 21005-5066

---

---

**ARL-TR-5224**

**June 2010**

---

## **Experimental Measurement and Computational Simulation of the Strains on a Single Yarn in a Kevlar Fabric During Stretching**

**Jian H. Yu, Brandon McWilliams,  
Peter G. Dehmer, and Chian-Fong Yen  
Weapons and Materials Research Directorate, ARL**

<b>REPORT DOCUMENTATION PAGE</b>			<i>Form Approved</i> <b>OMB No. 0704-0188</b>		
Public reporting burden for this collection of information is estimated to average 1 hour per response, including the time for reviewing instructions, searching existing data sources, gathering and maintaining the data needed, and completing and reviewing the collection information. Send comments regarding this burden estimate or any other aspect of this collection of information, including suggestions for reducing the burden, to Department of Defense, Washington Headquarters Services, Directorate for Information Operations and Reports (0704-0188), 1215 Jefferson Davis Highway, Suite 1204, Arlington, VA 22202-4302. Respondents should be aware that notwithstanding any other provision of law, no person shall be subject to any penalty for failing to comply with a collection of information if it does not display a currently valid OMB control number. <b>PLEASE DO NOT RETURN YOUR FORM TO THE ABOVE ADDRESS.</b>					
<b>1. REPORT DATE (DD-MM-YYYY)</b> June 2010		<b>2. REPORT TYPE</b> Final		<b>3. DATES COVERED (From – To)</b>	
<b>4. TITLE AND SUBTITLE</b> Experimental Measurement and Computational Simulation of the Strains on a Single Yarn in a Kevlar Fabric During Stretching				<b>5a. CONTRACT NUMBER</b>	
				<b>5b. GRANT NUMBER</b>	
				<b>5c. PROGRAM ELEMENT NUMBER</b>	
<b>6. AUTHOR(S)</b> Jian H. Yu, Brandon McWilliams, Peter G. Dehmer, and Chian-Fong Yen				<b>5d. PROJECT NUMBER</b>	
				<b>5e. TASK NUMBER</b>	
				<b>5f. WORK UNIT NUMBER</b>	
<b>7. PERFORMING ORGANIZATION NAME(S) AND ADDRESS(ES)</b> U.S. Army Research Laboratory ATTN: RDRL-WMM-B Aberdeen Proving Ground, MD 21005				<b>8. PERFORMING ORGANIZATION REPORT NUMBER</b> ARL-TR-5224	
<b>9. SPONSORING/MONITORING AGENCY NAME(S) AND ADDRESS(ES)</b>				<b>10. SPONSOR/MONITOR'S ACRONYM(S)</b>	
				<b>11. SPONSOR/MONITOR'S REPORT NUMBER(S)</b>	
<b>12. DISTRIBUTION/AVAILABILITY STATEMENT</b> Approved for public release; distribution unlimited.					
<b>13. SUPPLEMENTARY NOTES</b>					
<b>14. ABSTRACT</b> The ability to measure the strain on an individual yarn is essential for the understanding of mechanical properties of fabrics. Using a non-contact technique called photogrammetry, we investigate the deformation of a single yarn in a Kevlar® fabric as it undergoes stretching. Photogrammetry uses two charge-coupled device (CCD) cameras fitted with macro lenses to record stereo images of the fabric during stretching. We tracked the change in the arc length between a set of points and calculated the strain from the arc length at various locations. We used a finite element method (FEM) model to simulate the experiment, optimizing the material parameters in the FEM model by comparing the experimental data to the computational results. After optimization, the simulated displacement and strain time histories matched reasonably well with the experimental data.					
<b>15. SUBJECT TERMS</b> Photogrammetry strain measurements optical technique Kevlar fabric yarn					
<b>16. SECURITY CLASSIFICATION OF:</b>			<b>17. LIMITATION OF ABSTRACT</b> UU	<b>18. NUMBER OF PAGES</b> 18	<b>19a. NAME OF RESPONSIBLE PERSON</b> Jian H. Yu
<b>a. REPORT</b> Unclassified	<b>b. ABSTRACT</b> Unclassified	<b>c. THIS PAGE</b> Unclassified			<b>19b. TELEPHONE NUMBER (Include area code)</b> (410) 306-0698

Standard Form 298 (Rev. 8/98)  
Prescribed by ANSI Std. Z39.18

---

## Contents

---

<b>List of Figures</b>	<b>iv</b>
<b>1. Introduction</b>	<b>1</b>
<b>2. Experimental Method</b>	<b>1</b>
<b>3. Experimental Results</b>	<b>3</b>
<b>4. Finite Element Modeling</b>	<b>5</b>
<b>5. Comparison of Experimental and Modeling Results</b>	<b>7</b>
<b>6. Conclusions</b>	<b>9</b>
<b>7. References</b>	<b>10</b>
<b>Distribution List</b>	<b>11</b>

---

## List of Figures

---

Figure 1. The push-rod assembly and the steel frame. ....	2
Figure 2. The field-of-view of the fabric in the steel frame, showing the three sets of points on the yarn for tracking the displacement on yarn crossover #2. ....	3
Figure 3. The $x$ -, $y$ -, and $z$ -displacements at applied forces of 0, 110, and 438 N, respectively. ....	4
Figure 4. Average strains along the principal yarn at the crossovers; the error bar is the standard deviation from the mean strain. ....	5
Figure 5. (a) FEM mesh of the fabric and (b) the yarn dimensions. ....	6
Figure 6. Comparison of experimental and modeling results: $E_{11}$ modulus sensitivity (frictionless case). ....	8
Figure 7. Comparison of experimental and modeling results: strains at the principal yarn crossovers (friction coefficient = 0.25). ....	9

---

## 1. Introduction

---

The use of woven Kevlar fabric is prevalent in many applications, such as body armor, helmets, and composite structures. The performance of these fabrics is influenced by yarn material properties, yarn geometry, yarn architecture, boundary conditions, crimping, friction, etc. The ability to measure the strain on an individual yarn can provide insight into the yarn-to-yarn interactions within a fabric. Photogrammetric analysis has been used to measure the deformability of fabrics and textile composites. For instance, Lomov et al. (1, 2) studied the in-plane deformation of yarns in a fabric that underwent shearing using two-dimensional (2-D) photogrammetry. Non-optical techniques have also been used to measure the strain in yarns. In one case, Chocron et al. (3) wove a nickel-chromium wire that can measure strain into a fabric. In this report, we present a three-dimensional (3-D) photogrammetric analysis of a Kevlar fabric that has been subjected to a push-rod stretching test.

Computational (or finite element method [FEM]) models have been used to analyze ballistic impact on fabrics. Cheeseman (4), Duan (5, 6), Lim (7), and Talebi (8) used 3-D FEM solid elements to simulated fabrics impacted by projectiles of various geometries and confined under different boundary conditions. A fabric membrane model was developed by Yen (9) to lower the computation cost with a minimal reduction in accuracy. Most the aforementioned models need to be validated and the input parameters need to be optimized. We present an approach to optimize a constitutive model of a Kevlar fabric. We use experimental results to validate the FEM model and identify the sensitivity of the friction coefficient between yarns under a static stretching condition.

---

## 2. Experimental Method

---

We used a 5x5 plain-weave Kevlar fabric in the stretching test (5 warp yarns per inch and 5 weft yarns per inch, 12105 denier yarn, areal density = 530 g/m<sup>2</sup>). The fabric was clamped to a steel frame that had a circular opening diameter of 5.08 cm (figure 1). The push rod had a 1.905-cm-diameter brass ball attached to the end of the rod. We measured the applied force with an in-line load cell and used a screw rod to provide the forward movement (in the  $z$ -direction) of the push rod. To track displacement, we painted the surface of the fabric facing the cameras with a random dot pattern using black pen ink. Two charge-coupled device (CCD) cameras (Photron SA1, Photron USA, Inc.) were employed to generate stereo images of the deforming fabric. The cameras were placed behind the target fixture along the  $z$ -direction and the angle between of the cameras was set at 20°. The images were recorded at a 512×512 pixel resolution with a 1/60 s exposure on each frame. Each camera used a macro lens (Nikon AF-

Nikkor) with a focal length of 85 mm and a f-stop of f/8. The field of view was about 5 x 5 cm, centered on the location of the push-rod ball point. We saved the images as 8-bit TIFF files and analyzed them using a commercially available photogrammetric software program called ARAMIS (GOM GmbH, Germany, distributed by Trilion Quality Systems in the United States). ARAMIS has a built-in algorithm for calculating the displacement (the ARAMIS default settings are 15×13 facets × step, which is a standard calculation). The displacement sensitivity was at least 1.7 microns (10).

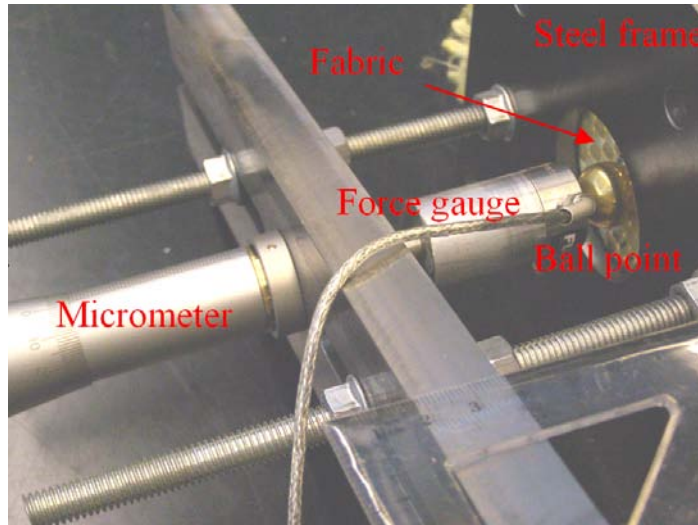


Figure 1. The push-rod assembly and the steel frame.

The displacement on a particular yarn crossover was tracked based on a set of points. The strain was calculated using the arc length across a set of four points (equation 1):

$$\varepsilon = \ln\left(\frac{l}{l_0}\right) \quad (1)$$

where  $\varepsilon$  is the strain,  $l$  is the deformed arc length, and  $l_0$  is the undeformed arc length. The deformed arc length is calculated using equation 2:

$$l = \sum (\Delta x^2 + \Delta y^2 + \Delta z^2)^{1/2} \quad (2)$$

where  $\Delta x$ ,  $\Delta y$ , and  $\Delta z$  are the displacements between the tracking points. The average strain on the yarn crossover is an average from three sets of tracking points (figure 2). The initial arc length is about 3.5 mm. The axes shown are the global coordinates. The tracking points are along the yarn axis, which is not necessarily parallel to the global  $x$ -axis.

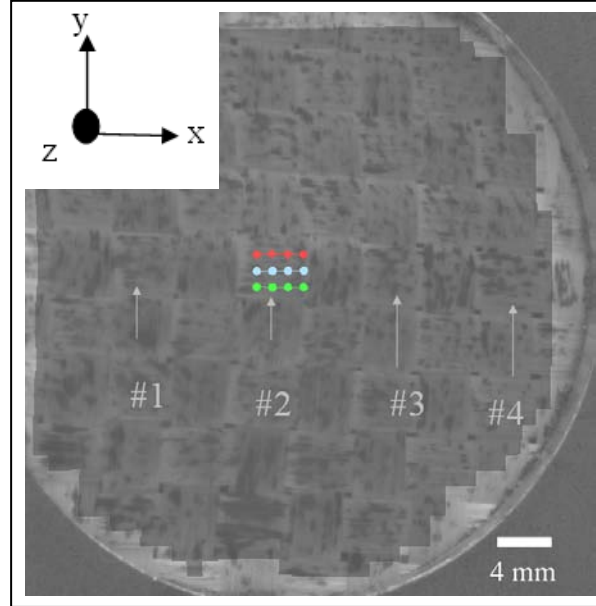


Figure 2. The field-of-view of the fabric in the steel frame, showing the three sets of points on the yarn for tracking the displacement on yarn crossover #2.

---

### 3. Experimental Results

---

We collected photogrammetric data to determine the fabric deflection as a function of the applied force. Figure 3 shows a full-field measurement of the  $x$ -,  $y$ -, and  $z$ -displacements of the fabric during stretching. The displacement plots indicate that the principal warp and weft, the yarns that were directly engaged by the push rod, experienced a higher stretching ratio than the secondary yarns. The contour lines illustrate that the fabric response is not isotropic; the greatest displacement gradients are along the weft and warp directions. The deformed fabric takes on a shape of a square pyramid with its corners along the warp and weft directions. This shape is similar to the shape of a deformed fabric that has been impacted by a high-speed projectile. Under static stretching conditions, the corners of the pyramid extend to the boundary of the circular clamp. However, during an impact event, the corners of the pyramid move toward the boundary.

A full-field strain tensor cannot be evaluated using the deformation gradient derived from the displacement vectors in this experiment. Fabric is not a rigid body. There are crimps in the yarn that can straighten out before the yarn is actually strained. Also, one yarn can slip past other yarns creating a false indication of strain. The best method for calculating strain is to track the changes in the arc length at the yarn's crossovers.

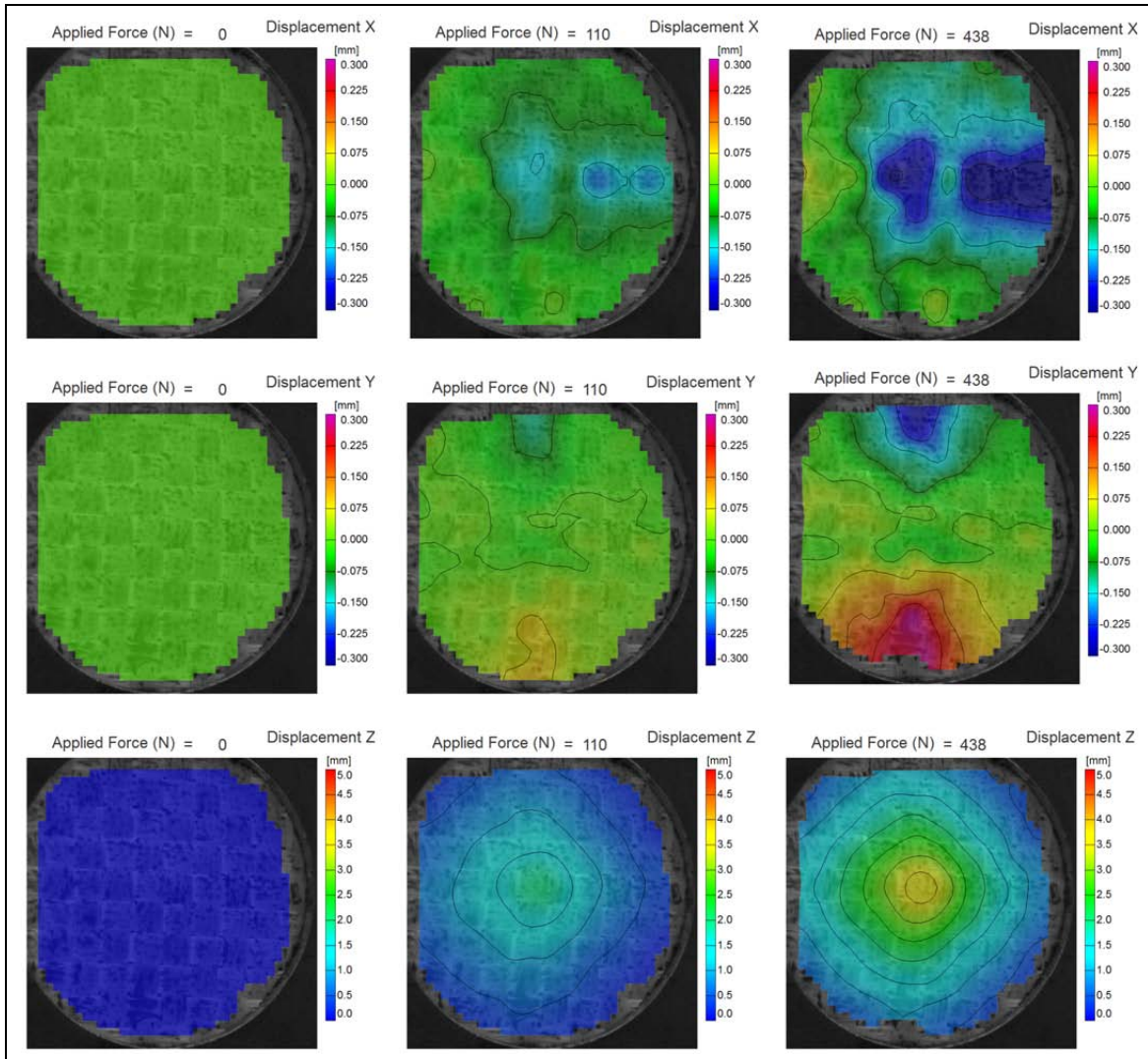


Figure 3. The  $x$ -,  $y$ -, and  $z$ -displacements at applied forces of 0, 110, and 438 N, respectively.

Figure 4 shows the calculated average strain along the principal yarn at various locations. At low applied forces, the calculated strain values are very noisy. This effect is due to the displacement sensitivity limit of the instrument. According to the ARAMIS manufacturer, the instrument's sensitivity is  $\sim 0.002$  mm for a field of view of  $50 \text{ mm}^2$  (10).

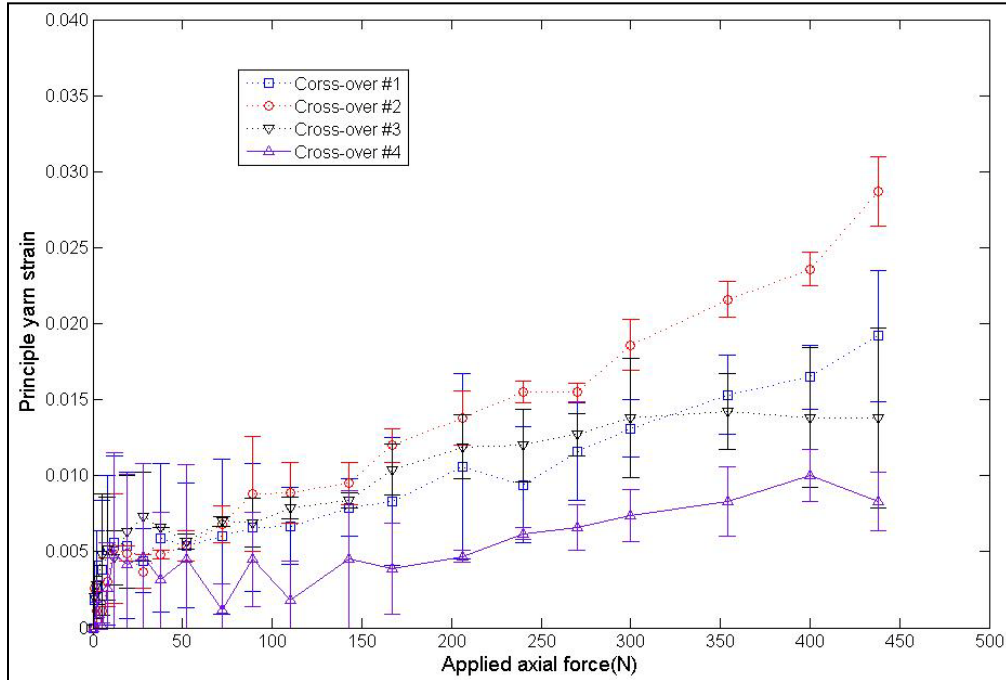


Figure 4. Average strains along the principal yarn at the crossovers; the error bar is the standard deviation from the mean strain.

The strain plots indicate that the strains along the yarn are not uniform. The highest strain is located near the contact point between the push rod and the fabric; the lowest strain is near the clamp boundary. The loads are not transmitted uniformly along the yarn. The yarn is pinned between the crossovers and the frictional force that interlocks the crossovers constricts the movement of the weft yarn, preventing strain relief from the relaxed section to the location where the yarn is already under strain. Once the applied force overcomes the frictional force at the crossovers, yarns can slip past each other, allowing the principal yarn to uncrimp and provide strain relief. The crossover near the push rod on the principal weft yarn experiences the highest strain among the crossovers. The loading is attenuated from the point of contact with the push rod to the boundary of the clamp, which indicates that some of the loading is being borne by the secondary yarns between the crossovers.

---

#### 4. Finite Element Modeling

---

The fabric model used here is a yarn-level FEM model based on a ballistic model from an earlier work (9). Computations were performed using the ABAQUS/Explicit software package. The yarns are represented by membrane (no bending stiffness) elements to reduce computation time, and the yarns in the fabric are simplified to plane segments (figure 5).

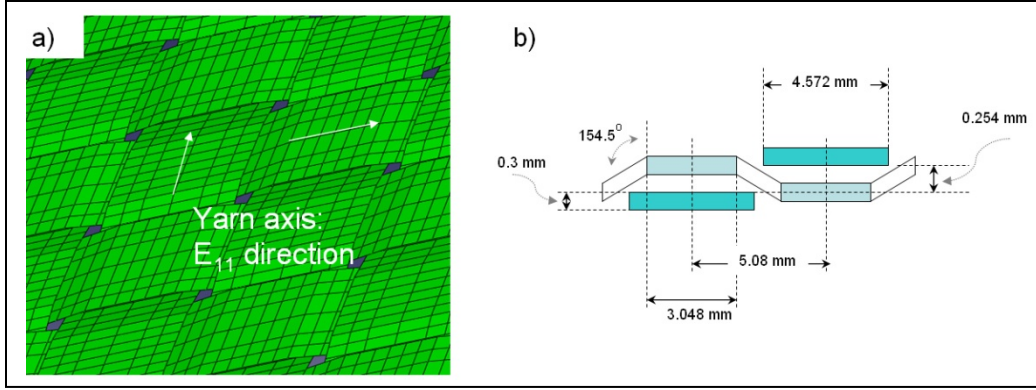


Figure 5. (a) FEM mesh of the fabric and (b) the yarn dimensions.

An orthotropic elastic constitutive model is used to describe the yarns:

$$\begin{bmatrix} \varepsilon_{11} \\ \varepsilon_{22} \\ \varepsilon_{33} \\ \varepsilon_{23} \\ \varepsilon_{31} \\ \varepsilon_{12} \end{bmatrix} = \begin{bmatrix} \frac{1}{E_{11}} & -\frac{\nu}{E_{22}} & -\frac{\nu}{E_{33}} & 0 & 0 & 0 \\ -\frac{\nu}{E_{11}} & \frac{1}{E_{22}} & -\frac{\nu}{E_{33}} & 0 & 0 & 0 \\ -\frac{\nu}{E_{11}} & -\frac{\nu}{E_{22}} & \frac{1}{E_{33}} & 0 & 0 & 0 \\ 0 & 0 & 0 & \frac{1}{2G} & 0 & 0 \\ 0 & 0 & 0 & 0 & \frac{1}{2G} & 0 \\ 0 & 0 & 0 & 0 & 0 & \frac{1}{2G} \end{bmatrix} \begin{bmatrix} \sigma_{11} \\ \sigma_{22} \\ \sigma_{33} \\ \sigma_{23} \\ \sigma_{31} \\ \sigma_{12} \end{bmatrix} \quad (3)$$

where  $\varepsilon$  is the strain,  $\sigma$  is the stress,  $E$  is the Young's modulus,  $G$  is the shear modulus, and  $\nu$  is the Poisson ratio. The yarns are oriented such that the fiber axis is the 11 direction. In actuality, each yarn consists of a bundle of fibers, which could be considered transversely isotropic. However, since we are using a continuum model at the yarn level, the moduli in all other directions, including the shear moduli, are assumed to be two orders of magnitude smaller than the principal yarn direction (9). Note: The modulus used here is an effective modulus,  $E_{11}^*$ , where  $E_{11}^* < E^{\text{fiber}}$ . This is due to the density of the yarn being less than the density of the base material due to the packing of the fibers. Poisson effects are assumed to be negligible and a small Poisson ratio of 0.001 is used.

A fixed boundary condition is applied to the yarn at the edge of the circular frame. The push rod is modeled as a rigid body. The value for the dynamic and static friction coefficients between the push rod and the fabric is 0.36 (11) and the friction coefficient,  $\mu_s$ , between the yarns is set to 0.25. Since there is uncertainty in  $E_{11}^*$ , due to difficulties in measuring the actual

density of the yarn and local variations in the fiber packing, a parametric study of for  $E_{11}^*$  was used to determine this effect on the fabric's response. An optimized effective modulus,  $E_{11}^*$ , was determined by comparing the experimental data to the modeling results.

---

## 5. Comparison of Experimental and Modeling Results

---

Figure 6 compares the experimental and modeling results of the applied force as a function of fabric displacement for the frictionless case. If the value of  $E_{11}$  is set too high, the fabric is too rigid. On the other hand, if  $E_{11}$  is set too low, the fabric is too compliant. There is an optimum value for  $E_{11}$  in which the modeling results are in reasonable agreement with the experimental results. Root mean square errors (RMSEs) were computed between the modeling values and the experimental curves for  $E_{11} = 35, 30,$  and  $25$  GPa. The RMSEs were 0.114, 0.048, and 0.106, respectively.  $E_{11} = 30$  GPa yielded the lowest RMSE; the force versus displacement profile was closely matched to the experiment data, especially in the low applied force (low displacement) region. RMSEs were also computed for  $\mu_s = 0, 0.25, 0.50,$  and  $0.75$  while setting  $E_{11} = 30$  GPa. The RMSEs were 0.048, 0.046, 0.046, and 0.048, respectively, indicating that the displacement was insensitive to the friction coefficient between the yarns. Unlike the case in dynamic impact, the yarns have time to redistribute their loads by slipping past each other at the crossovers during the static stretching.

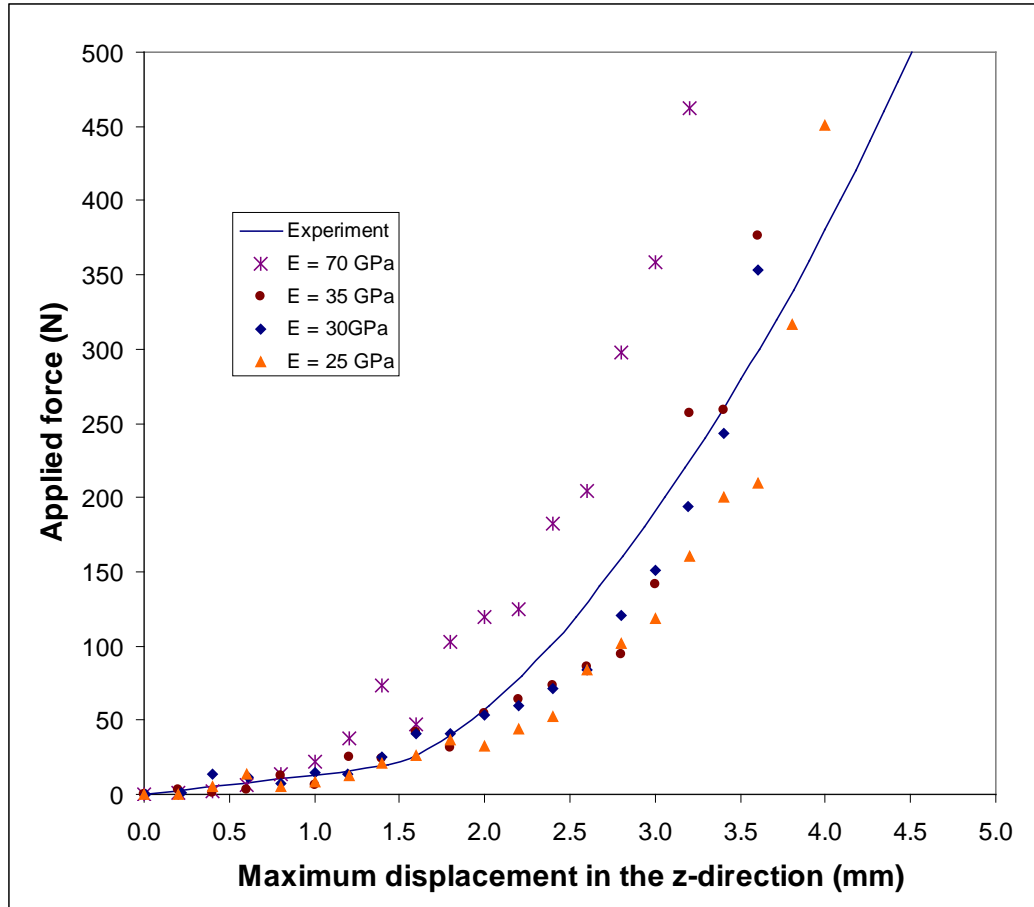


Figure 6. Comparison of experimental and modeling results:  $E_{11}$  modulus sensitivity (frictionless case).

There was a small discrepancy at the high applied force region where the modeled fabric showed more compliance than the actual fabric in the experiment. Instead of having a continuous curvature, the modeled yarns actually had a large crimping angle of  $154.5^\circ$ , which allowed the modeled yarns to have more yarn length to uncrimp than the actual yarn has. So, the modeled fabric had a higher deflection than the actual fabric at a given applied force.

The yarn strains at the crossovers are compared in figure 7 for  $E_{11} = 30$  GPa. Although the strain values are not exactly matched, the trend of increasing strain as a function of increasing applied force is in close agreement. The strain as function of the yarn crossover location also follows a similar trend: the strain increases from the fabric boundary to the area where the fabric is in direct contact with the push rod.

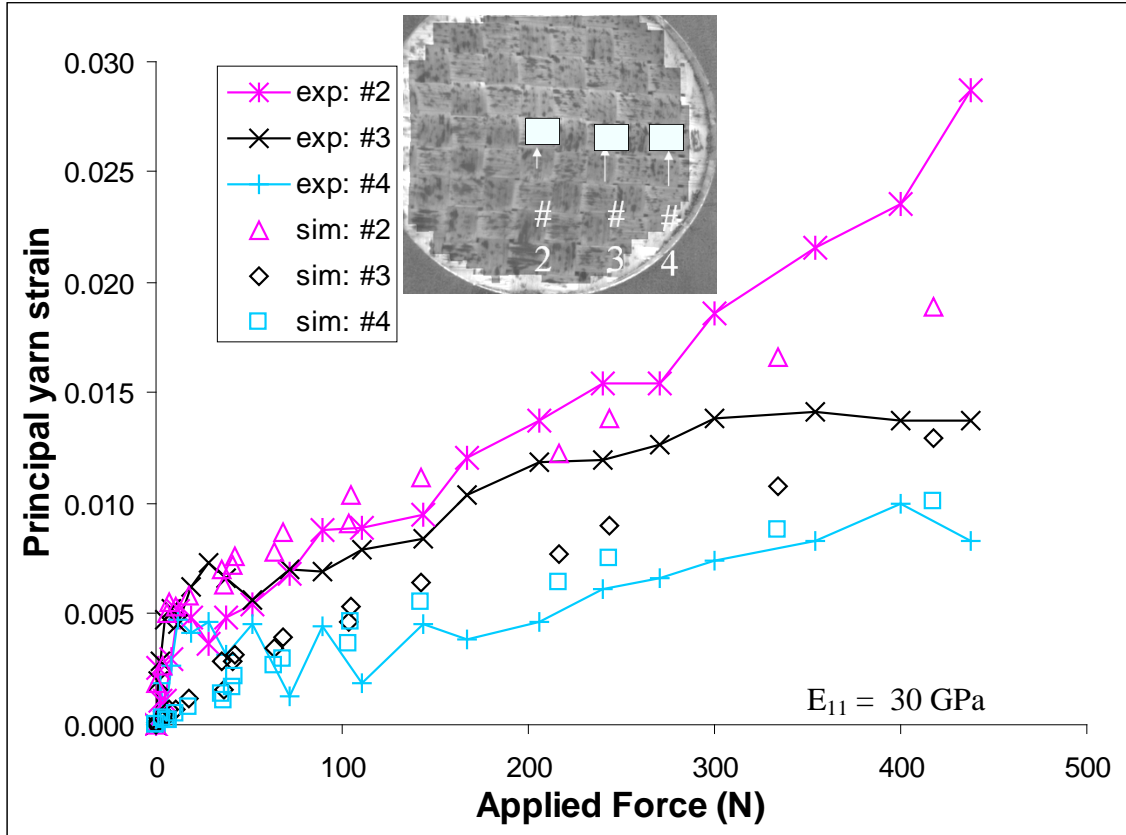


Figure 7. Comparison of experimental and modeling results: strains at the principal yarn crossovers (friction coefficient = 0.25).

## 6. Conclusions

In this study, we used photogrammetry to measure fabric stretching under static conditions. We successfully measured the local strain along a yarn in a fabric as it underwent stretching. The ability to measure the local strain on an individual yarn is a valuable tool for examining the mechanical behaviors of a fabric. We implemented a FEM model to simulate the experiment. The moduli in the FEM model were optimized by comparing the modeling results with the experimental data. After the optimization, the simulated displacement and strain time histories agreed reasonably well with the experimental data.

---

## 7. References

---

1. Lomov S. V.; et al. Full-field Strain Measurement for Validation of Meso-FE Analysis of Textile Composites. *Composites: Part A* **2008**, *39*, 1218–1231.
2. Lomov S. V.; et al. Full-field Strain Measurements in Textile Deformability Studies. *Composites: Part A* **2008**, *39*, 1232–1244.
3. Chocron, S.; et al. Measurement of Strain in Fabrics Under Ballistic Impact Using Embedded Nichrome Wires. Part I: Technique. *International J. of Impact Engineering* **2009**, *36*, 1296–1302.
4. Cheeseman, B. A.; Bogetti, T. A. Ballistic Impact Into Fabric and Compliant Composite Laminates. *Composite Structures* **2003**, *61*, 161–173.
5. Duan, Y.; et al. A Numerical Investigation of the Influence of Friction on Energy Absorption by a High-strength Fabric Subjected to Ballistic Impact. *International J. of Impact Engineering* **2006**, *32*.
6. Duan, Y.; et al. Finite Element Modeling of Transverse Impact on a Ballistic Fabric. *International Journal of Mechanical Sciences* **2006**, *48*, 33–43.
7. Lim, C. T.; Ng, Y. H.; Shim, V.P.W. Finite Element Modeling of the Ballistic Impact Into Fabric Armor. *International Journal of Impact Engineering* **2003**, *28*, 13–31.
8. Talebi, H.; Wong, S. V.; Hamouda, A.M.S. Finite Element Evaluation of Projectile Nose Angle Effects in Ballistic Perforation of High Strength Fabric. *Composite Structures* **2009**, *87*, 314–320.
9. Yen, C. F.; et al. Experimental Validation of a Kevlar Fabric Model for Ballistic Impact. *Proceedings of the 24<sup>th</sup> International Symposium on Ballistics*, New Orleans, LA, 2008, 51–58.
10. Schmidt, T.; et al. Full-field Dynamic Displacement and Strain Measurement Using Advanced 3D Image Correlation Photogrammetry: Part I. *Experimental Techniques* **May/June, 2003**, 47–50.
11. Orthwein, C. W. *Clutches and Brakes: Design and Selection Edition: 2, Illustrated*; CRC Press, ISBN 082474876X, 2004, p 9

No. of  
Copies Organization

- 1  
ELEC ADMNSTR  
DEFNS TECHL INFO CTR  
ATTN DTIC OCP  
8725 JOHN J KINGMAN RD STE 0944  
FT BELVOIR VA 22060-6218
- 3 US ARMY RSRCH LAB  
ATTN IMNE ALC HRR  
MAIL & RECORDS MGMT  
ATTN RDRL CIM L TECHL LIB  
ATTN RDRL CIM P TECHL PUB  
ADELPHI MD 20783-1197
- 1 US ARMY RSRCH LAB  
ATTN RDRL CIM G T LANDFRIED  
BLDG 4600  
ABERDEEN PROVING GROUND MD  
21005-5066
- 9 US ARMY RSRCH LAB  
ATTN RDRL WMM A  
R MERRILL  
E WETZEL  
ATTN RDRL WMM B  
B CHEESEMAN  
B MCWILLIAMS  
M VANLANDINGHAM  
C F YEN  
J YU  
ATTN RDRL WMM E  
P DEHMER  
ATTN RDRL WMM F  
B SCOTT  
BLDG 4600  
ABERDEEN PROVING GROUND MD  
21005-5066

TOTAL: 14 (1 ELEC, 13 HCS)

INTENTIONALLY LEFT BLANK.